Multifunctional Nanoparticles

DOI: 10.1002/ange.200805282

Gold Nanorod/Fe_3O_4 Nanoparticle "Nano-Pearl-Necklaces" for Simultaneous Targeting, Dual-Mode Imaging, and Photothermal Ablation of Cancer Cells**

*Chungang Wang, Jiji Chen, Tom Talavage, and Joseph Irudayaraj**

The combination of nanomaterials with different properties (such as magnetization, fluorescence, and near-infrared absorption) into one single object of nanoscale dimensions can lead to the development of multifunctional nanomedical platforms for simultaneous targeting, imaging, and therapy administration.[1] Of the various kinds of nanoparticles available, magnetic nanoparticles (MNPs) have been utilized as versatile probes in biomedical applications, because of their utility in magnetic resonance imaging (MRI).[2] Quantum dots (QDs) and fluorescent-dye-doped silica nanoparticles are representative examples of nanoparticles used in optical imaging.[3] In spite of their widespread use, fluorescent dyes are susceptible to photobleaching and quantum dots are difficult to functionalize in a controlled manner and are potentially toxic to cells, thus posing a concern for in vitro and in vivo applications. Recently, the photon luminescence effect of gold nanorods (Au_{rod}) has attracted much attention because of its excellent antiphotobleaching properties even under strong illumination and the chemically inert behavior of gold nanorods under physiological conditions, indicating that Au_{rod} could be used as an imaging agent.[4] Additionally, Au_{rod} have been shown to exhibit excellent therapeutic properties as hyperthermal agents since the local temperature around the Au_{rod} can be increased by laser illumination because of the tunable Au_{rod} surface plasmon bands in the near-infrared (NIR) region.[5] Among the various types of photothermal ablation technologies, NIR absorption photothermal therapy is particularly interesting because of the low scattering and low absorption by blood and soft tissue in this spectral region.[6] The combination of MRI diagnosis (up to 25–100 μm spatial resolution),[7] fluorescence imaging, and the NIR photothermal ablation (a few centimeters depth of penetration)[6,8] of targeted tumor cells would allow for multimodal imaging and photothermal therapy. Herein, we demonstrate a novel route to the synthesis of multifunctional nano-pearl-necklaces based on Fe_3O_4 nanoparticles decorating Au_{rod} that can be used as an MRI and fluorescence-imaging agent to target cancer cells. An additional function of photothermal therapy will also be demonstrated.

Figure 1 illustrates the fabrication of novel "nano-pearl-necklace" structured multifunctional nanoparticles comprising a single, amine-modified Au_{rod} decorated with multiple

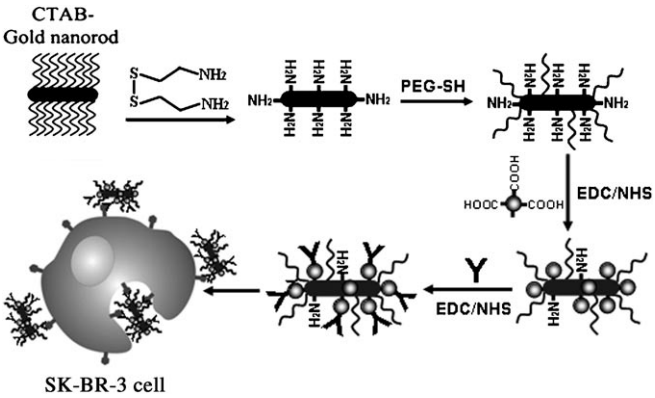

Figure 1. Schematic of synthesis and targeting of PEGylated Au_{rod}–Fe_3O_4 nano-pearl-necklace (Au_{rod}–$(Fe_3O_4)_n$) bioprobes for MRI, fluorescence imaging, and photothermal ablation of SK-BR-3 cells. black bar: gold nanorod, CTAB: cetyltrimethylammonium bromide, gray spheres: Fe_3O_4 nanoparticles, EDC/NHS: 1-ethyl-3-(3-dimethylaminopropyl)carbodiimide hychloride/*N*-hydroxysuccinimide, **Y**: Herceptin.

"pearls" of Fe_3O_4 nanoparticles capped with COOH groups. Then Au_{rod}–Fe_3O_4 nano-pearl-necklaces (abbreviated as Au_{rod}–$(Fe_3O_4)_n$, where $n > 5$) were further stabilized with thiol-modified poly(ethylene glycol) (SH-PEG, MW 5000) and functionalized with Herceptin as multifunctional bioprobes for targeting, dual-imaging, and photothermal killing of human breast cancer cells (SK-BR-3 cells).

Monodispersed 15 nm Fe_3O_4 nanoparticles (Figure 2A) bearing carboxy groups were synthesized by a previously described procedure.[9] Amine functionalized Au_{rod} with aspect ratio of approximately 3.6 were prepared using a seed-mediated surfactant-directed approach previously reported by Nikoobakht and El-Sayed[10] and in our previous work.[11] The resulting Au_{rod} were further stabilized with SH-PEG to obtain monodispersed nanoparticles (Figure 2B). Subsequently, the Au_{rod}–$(Fe_3O_4)_n$ probes were fabricated through the conjugation of PEGylated amine modified Au_{rod} with Fe_3O_4 nanoparticles capped with carboxy groups

[*] Dr. C. Wang,[+] J. Chen,[+] Dr. T. Talavage,[+] Prof. Dr. J. Irudayaraj
Birck Nanotechnology, Bindley Bioscience, and Purdue Cancer Center
Purdue University
225 S. University Street, West Lafayette, IN 47906 (USA)
Fax: (+86) 765-496-1115
E-mail: josephi@purdue.edu

[+] These authors contributed equally to this work.

[**] Part funding of this research from the CFSE-USDA grant is a gratefully acknowledged. A. Wang is acknowledged for providing magnetic nanoparticles from Ocean Nanotech LLC. Dr. Shalev is acknowledged for the temperature device.

Supporting information for this article is available on the WWW under http://dx.doi.org/10.1002/anie.200805282.

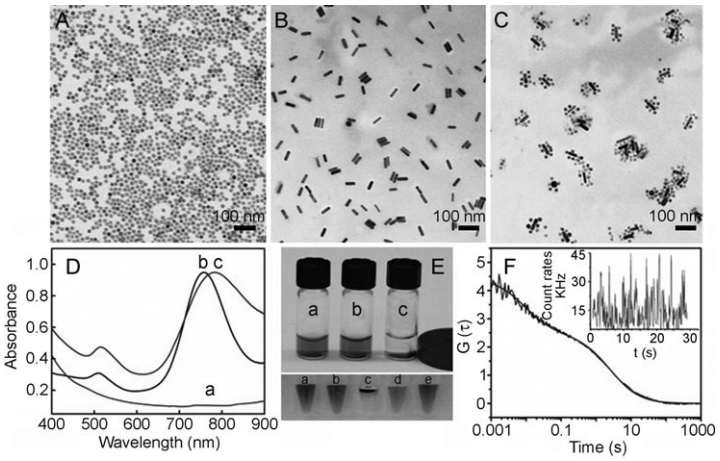

Figure 2. Transmission electron microscopic (TEM) images of A) COOH modified Fe_3O_4 nanoparticles, B) NH_2 modified Au_{rod}, C) Fe_3O_4 nanoparticles assembled onto the surface of Au_{rod} stabilized by PEG (Au_{rod}–$(Fe_3O_4)_n$). D) UV/Vis-NIR absorption spectra (a–c) corresponding to samples (A–C). E) top: photograph of nanoparticles in water in the presence of an external magnet (a–c) corresponding to (A–C), and bottom: photograph of Au_{rod}–$(Fe_3O_4)_n$ in different solvents a) PBS, b) ethanol, c) cloroform, d) DMSO, e) 1 M NaCl. F) Autocorrelation curve from fluorescence correlation spectroscopy (FCS) and photon lumination fluctuation trace (inset) measured from Au_{rod}–$(Fe_3O_4)_n$ in water.

using EDC/NHS chemistry (see Figure 1). Figure 2C shows the corresponding TEM image of Au_{rod} decorated with several Fe_3O_4 nanoparticles constituting the Au_{rod}–$(Fe_3O_4)_n$ probe. Figure 2D a–c show the UV/Vis-NIR spectra of carboxylated magnetic nanoparticles, PEGylated amine-modified Au_{rod}, and PEGylated Au_{rod}–$(Fe_3O_4)_n$. The PEGylated amine-modified Au_{rod} has a weak transverse plasmon (TP) band at 520 nm and a strong longitudinal plasmon (LP) band at 765 nm (Figure 2D b). After functionalization with Fe_3O_4 nanoparticles, the LP band is red-shifted from 765 nm to 785 nm and broadened (Figure 2D c) reflecting a change in the local dielectric field resulting from the presence of Fe_3O_4 nanoparticles. Photographs in Figure 2E a–c illustrate the effective separation of PEGylated Au_{rod}–$(Fe_3O_4)_n$ in the presence of an external magnet. PEGylated Au_{rod}–$(Fe_3O_4)_n$ are much more easily separable by a magnet than free Fe_3O_4 nanoparticles because more magnetic nanoparticles are attached, the free Fe_3O_4 nanoparticles only respond weakly. Dynamic light scattering (DLS) measurement revealed that the hydrodynamic size of PEGylated Au_{rod}–$(Fe_3O_4)_n$ in water was approximately 87 nm (Figure S1 in the Supporting Information), suggesting no apparent aggregation. The ability to vary the number of magnetic particles around a nanorod provides a magnetically tunable Au_{rod}–$(Fe_3O_4)_n$ probe that can be used for ultra-sensitive MR diagnostic imaging.

Once fabricated, first the Au_{rod}–$(Fe_3O_4)_n$ nanoprobes, are separated from the unattached Au_{rod} by an external magnet, then the free magnetic nanoparticles are removed by low-speed centrifugation. The Au_{rod}–$(Fe_3O_4)_n$ nanoprobes were found to be stable in different solvents (phosphate buffer solution (PBS), pH 7.4, ethanol, chloroform, and DMSO) as well as in concentrated salt (1M) solution (Figure 2E (bottom)). Interestingly, the Au_{rod}–$(Fe_3O_4)_n$ also transfer partially into an organic phase in a chloroform–water system.

Fluorescence correlation spectroscopy (FCS), an ultrasensitive and non-invasive single-molecule technique generally used to study single-molecule diffusion and provide information on the number of molecules in a confocal volume (ca. femtoliter (fL)) by autocorrelating the fluorescence signal of the diffusers, was used to study the efficiency of these probes as a labeling and a targeting agent at single-molecule resolution. The diffusion characteristics of Au_{rod}–$(Fe_3O_4)_n$ from the autocorrelation curve was fitted by a free 3D diffusion model[12] and the diffusion time was estimated to be 3.1 ms (Figure 2F). A typical count rate trace, depicting the fluctuation of Au_{rod} fluorescence intensity in real time (Figure 2F, inset), suggests that these probes are stable and do not photobleach, ensuring their utility in imaging and single- molecule experiments.

The utility of Herceptin-tagged Au_{rod}–$(Fe_3O_4)_n$ was demonstrated in dual-mode imaging and photothermal ablation of SK-BR-3 breast cancer cells overexpressing the human epidermal growth factor receptor 2 (HER-2). The remaining carboxy groups provided by Fe_3O_4 nanoparticles in Au_{rod}–$(Fe_3O_4)_n$ were conjugated with Herceptin, which is a humanized IgG monoclonal antibody directed against the extracellular domain of the HER-2 receptor.[13] First the cytotoxic behavior of Au_{rod}–$(Fe_3O_4)_n$ and Au_{rod}–$(Fe_3O_4)_n$–Herceptin conjugates on SK-BR-3 cells was examined by the MTT (3-(4,5-dimethylthiazol-2-yl)-2,5-diphenyltetrazolium bromide) assay. As expected, the Au_{rod}–$(Fe_3O_4)_n$ nanoparticles were reasonably nontoxic and biocompatible, whereas Au_{rod}–$(Fe_3O_4)_n$–Herceptin conjugates show a dose-dependent toxicity. Thus, no obvious cytotoxicity was observed at lower doses, while higher doses exhibited some toxicity was detected; Herceptin is known to have an anti-proliferative effect on HER-2 expressing cells[14] (Figure S2 in the Supporting Information).

To demonstrate the potential use as an enhanced MRI contrast agent, Au_{rod}–$(Fe_3O_4)_n$ was compared to bare Fe_3O_4 nanoparticles of an equivalent iron concentration. MR images were obtained using a clinical 3.0-T MR system. The free Fe_3O_4 nanoparticles show a weak MR contrast with a r_2 relaxivity value of 63.5 $mM^{-1}s^{-1}$, however, Fe_3O_4 nanoparticles decorating the gold nanorods, Au_{rod}–$(Fe_3O_4)_n$, exhibited a remarkably stronger MR contrast with a dramatically increased r_2 value of 248.1 $mM^{-1}s^{-1}$ (Figure 3A and Figure S3 in the Supporting Information). The significant improvement in the MR signal could be attributed to the synergistic magnetic effect of multiple Fe_3O_4 nanoparticles surrounding a core Au_{rod} that result in magnetic coupling between Fe_3O_4 nanoparticles.[15] These results suggest that the Au_{rod}–$(Fe_3O_4)_n$ has a stronger magnetization than free Fe_3O_4 nanoparticles and could serve as more effective contrast agents for MRI imaging of breast cancer cells. In Figure 3B (top), the T_2-weighted MR images for the untreated SK-BR-3 cells (a), the Au_{rod}–$(Fe_3O_4)_n$–Herceptin conjugates treated HER-2^- MCF-7 cells (b), and Au_{rod}–$(Fe_3O_4)_n$ treated HER-2^+ SK-BR-3 cells as a control are shown. The Au_{rod}–$(Fe_3O_4)_n$–Herceptin con-

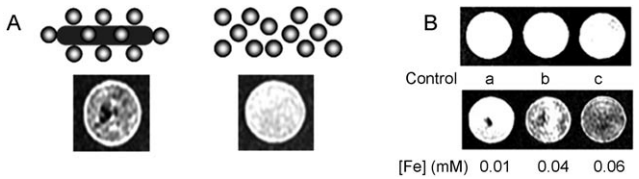

Figure 3. A) Synergistic MR enhancement effect of Au_{rod}–Fe_3O_4 nanoprobes. T_2-weighted MR images of Au_{rod}–Fe_3O_4–Herceptin nanoprobes (left) and free Fe_3O_4 nanoparticles (right). B) top: T_2-weighted MR images of untreated SK-BR-3 cells, b) MCF-7 cells treated with Au_{rod}–$(Fe_3O_4)_n$–Herceptin nanoprobes, and c) SK-BR-3 cells treated with Au_{rod}–$(Fe_3O_4)_n$; bottom: T_2-weighted MR images of SK-BR-3 cells treated with Au_{rod}–$(Fe_3O_4)_n$–Herceptin nanoprobes at different concentrations.

jugates treated MCF-7 cells and control SK-BR-3 cells exhibited extremely weak MR signals as shown in Figure 3B (top; a, b, and c). The T_2-weighted MR images of the Au_{rod}–$(Fe_3O_4)_n$–Herceptin conjugated probes targeting HER-2^+ overexpressing SK-BR-3 cells show a much darker contrast as the probe concentration increased (Figure 3B, bottom).

The targeting specificity of Au_{rod}–$(Fe_3O_4)_n$–Herceptin nanoprobes for SK-BR-3 cells was assessed by the intracellular uptake of this nanoprobe compared to non-targeting nanoprobes as a control. A pronounced difference between the targeted and untargeted (that is, bare) nanoprobes against SK-BR-3 cells was noted. The change may be attributed to the ligand–receptor-mediated nanoprobe internalization by targeted cells.

By taking advantage of the inherent fluorescence of Au_{rod}, fluorescent images from the Au_{rod}–$(Fe_3O_4)_n$ probes were also obtained. The photon illumination confocal image of SK-BR-3 cells incubated with Au_{rod}–$(Fe_3O_4)_n$–Herceptin conjugates (Figure 4A) shows that some probes were bound to the cell surface and internalized into cytoplasma through specific binding to HER-2 overexpressing SK-BR-3 cells. Meanwhile, to further confirm that Au_{rod}–$(Fe_3O_4)_n$–Herceptin probes were specifically endocytozed by the SK-BR-3 cells, control experiments were performed using MCF-7 cells under these conditions. As expected, the nonspecific binding and the presence of endocytozed Au_{rod}–$(Fe_3O_4)_n$ probes when MCF-7 cells were used was insignificant (Figure 4B). Control experiments using SK-BR-3 cells incubated with bare Au_{rod}–$(Fe_3O_4)_n$ probes (i.e. without Herceptin) shows only the autofluorescence (Figure 4C), further confirming that these probes could be effecting labeling agents.

An autocorrelation plot of single nanoprobe (Figure 2F) diffusion using FCS (Figure 4D) shows that the intracellular diffusion time of Au_{rod}–$(Fe_3O_4)_n$ was 5.5 ms (compared to the free diffusion time of 3 ms from Figure 2F)). The longer diffusion time may possibly be due to the high density of the cellular microcosm. These results suggest that the targeted Au_{rod}–$(Fe_3O_4)_n$–Herceptin could be very useful in cancer diagnostics and research.

The aforementioned results were also consistent with the cellular uptake shown in TEM images (Figure 5). Targeting of SK-BR-3 cells using PEGylated Au_{rod}–$(Fe_3O_4)_n$–Herceptin nanoprobes (1 h incubation at 37°C) shows that a significant amount of Au_{rod}–$(Fe_3O_4)_n$–Herceptin localized in the cyto-

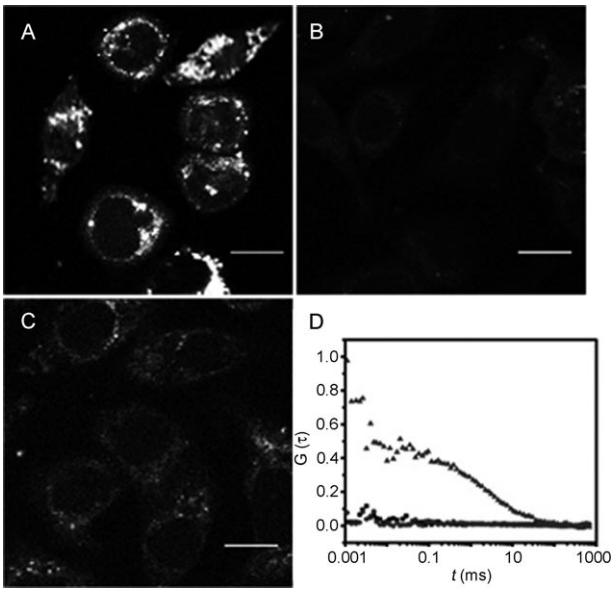

Figure 4. Photon lumination confocal images of A) SK-BR-3 and B) MCF-7 cells incubated with Au_{rod}–$(Fe_3O_4)_n$–Herceptin. C) SK-BR-3 cells incubated with Au_{rod}–$(Fe_3O_4)_n$ without Herceptin (control). D) Autocorrelation curves of FCS (▲), (●), and (■) corresponding to samples (A–C), respectively.

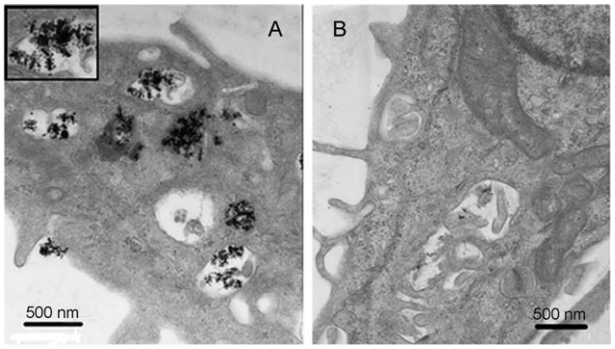

Figure 5. TEM images of SK-BR-3 cells incubated with A) Au_{rod}–$(Fe_3O_4)_n$–Herceptin (inset: An enlarged view of a representative sample section shows the Au_{rod}–$(Fe_3O_4)_n$–Herceptin nanoprobe uptake by a cell), B) Au_{rod}–$(Fe_3O_4)_n$.

plasmic vesicles (Figure 5A), while SK-BR-3 cells incubated with nanoprobes without Herceptin show no uptake for the same conditions (Figure 5B). These findings confirm that Herceptin-mediated endocytosis is a predominant mechanism for the uptake of PEGylated Au_{rod}–$(Fe_3O_4)_n$–Herceptin nanoprobes. More significantly, Figure 5A reveals that the Au_{rod}–$(Fe_3O_4)_n$–Herceptin nanoprobes maintain their original morphology and size within the cytoplasm of the cells assuring the integrity of these probes for multifunctional use. Effective internalization of the Au_{rod}–$(Fe_3O_4)_n$–Herceptin nanoprobes suggest that these probes can be used for targeting and as an inherent labeling agent. The integrity of these multifunctional probes further demonstrates that the controlled attachment of Fe_3O_4 nanoparticles around single Au_{rod} could serve as an effective MRI contrast agent.

To further confirm the feasibility of Au_{rod}–$(Fe_3O_4)_n$–Herceptin nanoprobes as photothermal therapy agents, NIR irradiation-induced temperature changes for Au_{rod}–$(Fe_3O_4)_n$ nanoprobes (0.2 and 1.2 nM based on Au nanorod) were investigated. Results show an average temperature increase of approximately 20 and 25 °C for 0.2 and 1.2 nM Au_{rod}–$(Fe_3O_4)_n$ respectively, within 5 min. In contrast, pure water had no apparent increase after being exposed to laser irradiation (4.53 W cm^{-2}) at the same condition (Figure S4 in the Supporting Information). These results show that Au_{rod}–$(Fe_3O_4)_n$ nanoprobes could be used as photothermal therapy agents.[16]

The HER-2 receptor is associated with homo and/or hetero dimerization of breast cancer cells by clustering on the plasma membrane. When Au_{rod}–$(Fe_3O_4)_n$–Herceptin nano probes bind to HER-2 receptors at the cell surface, receptor clustering is expected to induce a large amount of nanoparticle internalization and consequently its aggregation in the vesicles and cytoplasma, as observed from TEM images (Figure 5A). Effective internalization provides an opportunity to utilize the same probes for the selective destruction of SK-BR-3 cells upon irradiation by a 785 nm NIR laser. The cells were irradiated at a power density of 4.53 W cm^{-2} for 5 min. After exposure to the laser, the cells were incubated for an additional 2 h at 37 °C. To evaluate the cell viability, Calcein AM and Propidium Iodide (PI) were then used to stain living (green) and dead cells (red), respectively (Figure 6). SK-BR-3 cell death was observed when targeted by the Au_{rod}–$(Fe_3O_4)_n$–Herceptin probes (Figure 6A). On the other hand, Figure 6B and C shows that control SK-BR-3 cells incubated with unmodified Au_{rod}–Fe_3O_4 and MCF-7 cells incubated with Au_{rod}–$(Fe_3O_4)_n$–Herceptin survived after exposure to laser. These results clearly demonstrate that Au_{rod}–$(Fe_3O_4)_n$–Herceptin probes which can absorb NIR radiation, to effectively disrupt the targeted SK-BR-3 cells.

In conclusion, Herceptin-conjugated Au_{rod}–$(Fe_3O_4)_n$ nanoprobes were used to target SK-BR-3 cells. The multifunctional utility of the tumor targeting probes was successfully demonstrated by dual-mode imaging, single-nanoparticle intracellular dynamics monitoring, and photothermal ablation studies. The nanoprobes were shown to be magnetically and optically (in the NIR region) active and are therefore useful for simultaneous magnetic and optical detection. Further research on dual functionalization of these probes for targeted drug delivery and multimodal diagnostics in vivo is in progress.

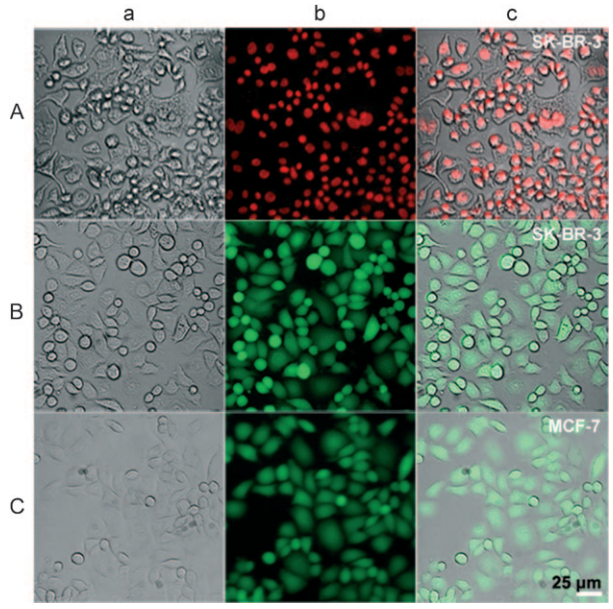

Figure 6. a) Transmission image, b) fluorescence image, and c) overlaid images of A) SK-BR-3 cells incubated with Au_{rod}–$(Fe_3O_4)_n$–Herceptin conjugates, irradiated, and subsequently stained with Propidium Iodide; B) SK-BR-3 cells incubated with Au_{rod}–$(Fe_3O_4)_n$ without Herceptin, irradiated, and subsequently stained with Calcein AM and, C) MCF-7 cells incubated with Au_{rod}–$(Fe_3O_4)_n$–Herceptin conjugates, irradiated, and subsequent staining with Calcein AM. Scale bar: 25 μm. In all the experiments irradiation was at a power density of 4.53 W cm^{-2} for 5 min.

Received: October 28, 2008
Revised: December 20, 2008
Published online: March 12, 2009

Keywords: cell recognition · gold · imaging agents · nanoparticles · photothermal ablation

[1] a) J. Kim, S. Park, J. E. Lee, S. M. Jin, J. H. Lee, I. S. Lee, I. Yang, J. S. Kim, S. K. Kim, M. H. Cho, T. Hyeon, *Angew. Chem.* **2006**, *118*, 7918; *Angew. Chem. Int. Ed.* **2006**, *45*, 7754; b) C. J. Xu, J. Xie, D. Ho, C. Wang, N. Kohler, E. G. Walsh, J. R. Morgan, Y. E. Chin, S. H. Sun, *Angew. Chem.* **2008**, *120*, 179; *Angew. Chem. Int. Ed.* **2008**, *47*, 173; c) M. Liong, J. Lu, M. Kovochich, T. Xia, S. G. Ruehum, A. E. Nel, F. Tamanoi, J. I. Zink, *ACS Nano* **2008**, *2*, 896; d) T. A. Larson, J. Bankson, J. Aaron, K. Sokolov, *Nanotechnology* **2007**, *18*, 325101; e) L. Y. Wang, J. W. Bai, Y. J. Li, Y. Huang, *Angew. Chem.* **2008**, *120*, 2473; *Angew. Chem. Int. Ed.* **2008**, *47*, 2439; f) H. Park, J. Yang, S. Seo, K. Kim, J. Suh, D. Kim, S. Haam, K. H. Yoo, *Small* **2008**, *4*, 192.

[2] a) J. H. Park, G. V. Maltzahn, L. L. Zhang, M. P. Schwartz, E. Ruoslahti, S. N. Bhatia, M. J. Sailor, *Adv. Mater.* **2008**, *20*, 1630; b) Y. W. Jun, J. H. Lee, J. W. Cheon, *Angew. Chem.* **2008**, *120*, 5200; *Angew. Chem. Int. Ed.* **2008**, *47*, 5122; c) J. H. Lee, Y. M. Huh, Y. Jun, J. Seo, J. Jang, H. T. Song, S. Kim, E. J. Cho, H. G. Yoon, J.-S. Suh, J. Cheon, *Nat. Med.* **2007**, *13*, 95; d) Y. W. Jun, J.-W. Seo, J. W. Cheon, *Acc. Chem. Res.* **2008**, *41*, 179; e) F. Q. Hu, L. Wei, Z. Zhou, Y. L. Ran, Z. Li, M. Y. Gao, *Adv. Mater.* **2006**, *18*, 2553.

[3] a) W. C. Chan, S. Nie, *Science* **1998**, *281*, 2016; b) M. Bruchez, Jr., M. Moronne, P. Gin, S. Weiss, A. P. Alivisatos, *Science* **2005**, *307*, 538; c) X. Michalet, F. F. Pinaud, L. A. Bentolila, J. M. Tsay, S. Doose, J. J. Li, G. Sundaresan, A. M. Wu, S. S. Gambhir, S. Weiss, *Science* **2005**, *307*, 538; d) K. M. Wang, S. Santra, X. J. Zhao, L. R. Hilliard, J. E. Smith, Y. R. Wu, W. H. Tan, *Anal. Chem.* **2006**, *78*, 646; e) W. H. Tan, K. M. Wang, X. X. He, X. J. J. Zhao, T. Drake, L. Wang, R. Bagwe, *Med. Res. Rev.* **2004**, *24*, 621.

[4] a) N. J. Durr, T. Larson, D. K. Smith, B. A. Korgel, K. Sokolov, A. Ben-Yakar, *Nano Lett.* **2007**, *7*, 941; b) H. F. Wang, T. B. Huff, D. A. Zweifel, W. He, P. S. Low, A. Wei, J. X. Cheng, *Proc. Natl. Acad. Sci. USA* **2005**, *102*, 15752; c) J. Park, A. Westrada, K. Sharp, K. Sang, J. A. Schwartz, D. K. Smith, C. Coleman, J. D. Payne, B. A. Korgel, *Opt. Exp.* **2008**, *16*, 1590.

[5] a) X. H. Huang, I. H. El-Sayed, W. Qian, M. A. El-Sayed, *J. Am. Chem. Soc.* **2006**, *128*, 2115; b) R. S. Norman, J. W. Stone, A. Gole, C. J. Murphy, T. L. Sabo-Attwood, *Nano Lett.* **2008**, *8*, 302;

c) L. Tong, Y. Zhao, T. B. Huff, M. N. Hansen, A. Wei, J. X. Chen, *Adv. Mater.* **2007**, *19*, 3136; d) D. Pissuwan, S. M. Valenzuela, C. M. Miller, M. B. Cortie, *Nano Lett.* **2007**, *7*, 3808; e) L. Hirsch, R. Stafford, J. Bankson, S. Sershen, B. Rivera, R. Price, J. Hazle, N. Halas, J. West, *Proc. Natl. Acad. Sci. USA* **2003**, *100*, 13549.
[6] R. Weissleder, *Nat. Biotechnol.* **2001**, *19*, 316.
[7] J. Cheon, J. H. Lee, *Acc. Chem. Res.* **2008**, *41*, 1630.
[8] P. K. Jain, I. H. El-Sayed, M. A. El-Sayed, *Nano Today* **2007**, *2*, 18.
[9] a) W. W. Yu, J. C. Falkner, C. T. Yavuz, V. L. Colvin, *Chem. Commun.* **2004**, 2306; b) C. J. Lin, R. A. Sperling, J. K. Li, T. Y. Yang, P. Y. Li, M. Zanella, W. H. Chang, W. J. Parak, *Small* **2008**, *4*, 334; c) X. H. Gao, Y. Cui, R. M. Levenson, L. W. K. Chung, S. M. Nie, *Nat. Biotechnol.* **2004**, *22*, 969.
[10] a) B. Nikoobakht, M. A. El-Sayed, *Chem. Mater.* **2003**, *15*, 1957.
[11] C. G. Wang, J. Irudayaraj, *Small* **2008**, *4*, 2204.
[12] L. T. Varghese, R. K. Sinha, J. Irudayaraj, *Anal. Chim. Acta* **2008**, *625*, 103.
[13] I. Steinhauser, B. Späjkuch, K. Strebhardt, K. Langer, *Biomaterials* **2006**, *27*, 4975.
[14] R. Nahta, F. J. Esteva, *Cancer Lett.* **2006**, *232*, 123.
[15] a) J.-F. Berret, N. Schonbeck, F. Gazeau, D. El Kharrat, O. Sandre, A. Vacher, M. Airiau, *J. Am. Chem. Soc.* **2006**, *128*, 1755; b) J. H. Lee, Y.-W. Jun, S.-I. Yeon, J. S. Shin, J. Cheon, *Angew. Chem.* **2006**, *118*, 8340; *Angew. Chem. Int. Ed.* **2006**, *45*, 8160.
[16] a) D. Coffey, R. Getzenberg, T. DeWeese, *JAMA J. Am. Med. Assoc.* **2006**, *296*, 445; b) E. Gabano, D. Colangelo, A. R. Ghezzi, D. Osella, *J. Inorg. Biochem.* **2007**, *98*, 73.

